Excitonic Resonant Emission–Absorption of Surface Plasmons in Transition Metal Dichalcogenides for Chip-Level Electronic–Photonic Integrated Circuits

Zhuan Zhu,[†,‡] Jiangtan Yuan,[§] Haiqing Zhou,[∥] Jonathan Hu,[⊥] Jing Zhang,[§] Chengli Wei,[⊥] Fang Yu,[∥] Shuo Chen,[∥] Yucheng Lan,[∥,#] Yao Yang,[§] Yanan Wang,[†,‡] Chao Niu,[⊥] Zhifeng Ren,[∥] Jun Lou,[§] Zhiming Wang,*,[†] and Jiming Bao*,[‡,†]

[†]Institute of Fundamental and Frontier Sciences, University of Electronic Science and Technology of China, Chengdu, Sichuan 610054, China

[‡]Department of Electrical and Computer Engineering and [∥]Department of Physics and Texas Center for Superconductivity, University of Houston, Houston, Texas 77204, United States

[§]Department of Materials Science and NanoEngineering, Rice University, Houston, Texas 77005, United States

[⊥]Department of Electrical & Computer Engineering, Baylor University, Waco, Texas 76798, United States

[#]Department of Physics and Engineering Physics, Morgan State University, Baltimore, Maryland 21251, United States

ABSTRACT: The monolithic integration of electronics and photonics has attracted enormous attention due to its potential applications. A major challenge to this integration is the identification of suitable materials that can emit and absorb light at the same wavelength. In this paper we utilize unique excitonic transitions in WS_2 monolayers and show that WS_2 exhibits a perfect overlap between its absorption and photoluminescence spectra. By coupling WS_2 to Ag nanowires, we then show that WS_2 monolayers are able to excite and absorb surface plasmons of Ag nanowires at the same wavelength of exciton photoluminescence. This resonant absorption by WS_2 is distinguished from that of the ohmic propagation loss of silver nanowires, resulting in a short propagation length of surface plasmons. Our demonstration of resonant optical generation and detection of surface plasmons enables nanoscale optical communication and paves the way for on-chip electronic–photonic integrated circuits.

KEYWORDS: 2D transition metal dichalcogenides, electronic–photonic integrated circuits, resonant exciton–plasmon interaction, chip-scale optical communication
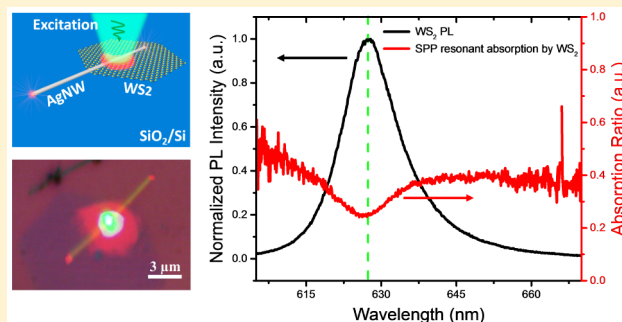
The emission and absorption of photons through electronic transitions is a basic light–matter interaction and forms the foundation for optoelectronic devices and optical telecommunications. Because optical emission and absorption originate from the same dipole transition matrix element in quantum mechanics, they are reversible and have the same magnitude in principle. In other words, if a photon is emitted by a quantum system, it should also be absorbed by the same system. Such emission–absorption resonance is a characteristic of two-level model systems and is ubiquitous in atomic spectra. However, such a resonance is hard to observe in conventional optical materials such as III–V semiconductors. In such a material, a photon is emitted at the band gap, but the absorption by the same material is virtually zero because the absorption increases as the square root of $E − E_g$, where E_g is the band gap. Such a resonance is also difficult to observe in semiconductor quantum dots, artificial atoms that exhibit atom-like discrete energy levels and absorption spectra: there is typically a significant red-shift of the emission peak relative to the absorption spectrum.[1] This Stokes shift is a general optical property of quantum dots; it cannot be eliminated simply by changing the size of quantum dots.[2–4] The resonance, however, can be achieved under certain conditions by carefully tuning the Fermi level of QDs with an electrical gating.[5]

The ability of an electronic material to emit and absorb photons at the same wavelength is essential to chip-scale optical communication and monolithic integration of electronic and photonic circuits, which would not only increase the speed of computation with reduced power consumption but also provide new applications such as quantum information processing and chemical or biological sensing.[6–9] The idea of an electronic–photonic integrated circuit (EPIC) dates back decades after the great successes of silicon microelectronics and fiber-based
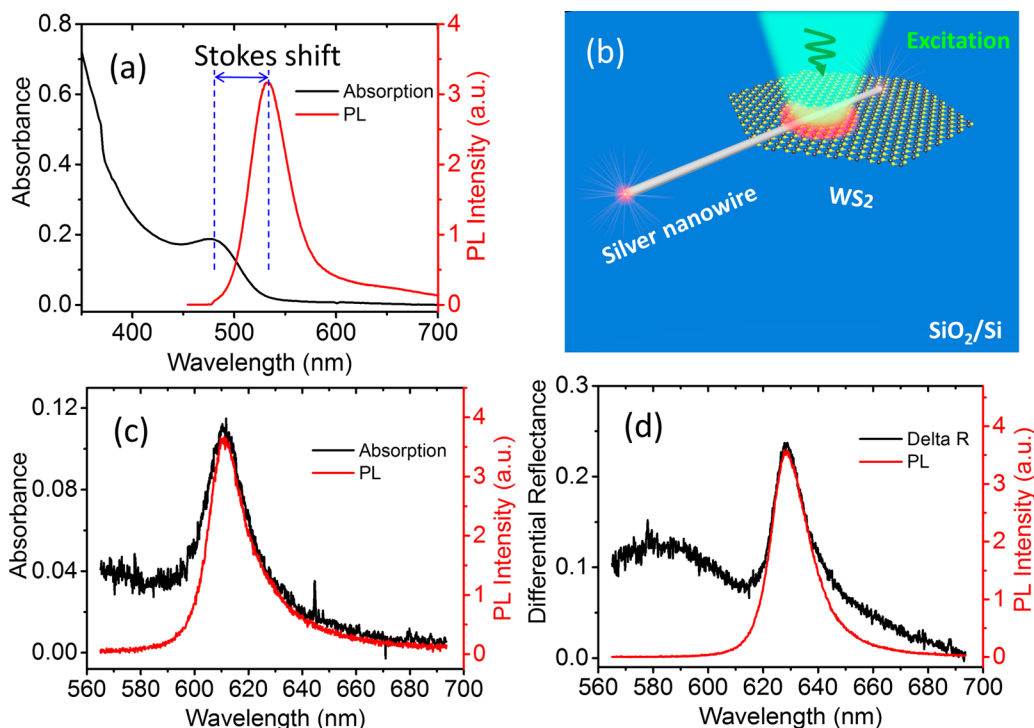
Figure 1. Photoluminescence, absorption, and experimental setup. (a) Photoluminescence and absorption spectra of CdTe quantum dots. (b) Experimental configuration showing the photoexcitation of WS$_2$ and the coupling between the Ag nanowire and WS$_2$. (c and d) Photoluminescence and absorption spectra of WS$_2$ monolayers on (c) a quartz and (d) a SiO$_2$/Si substrate. Differential reflectance is equivalent to the absorption spectrum for atomically thin films.

optical communications. Silicon is a natural choice of material for EPIC because of silicon-based mature electronics, but silicon is an indirect band gap semiconductor, which makes it challenging to use Si for efficient light generation and detection. In silicon photonics, much effort has been made to either transform silicon to an active optical material or integrate silicon with other optically active materials. Decades of research has culminated in the recent demonstration of a board-level EPIC.[10] However, that technique cannot be simply used to build a monolithic chip-level EPIC due to potential material incompatibility and scale mismatch between electronics and photonics. This nanometer versus micrometer scale mismatch problem has now been solved by the emergence of plasmonics, which enables confinement of light to a size compatible with electronics.[11−14] Much progress has since been made toward the chip-level EPIC. Falk et al. demonstrated local electrical detection of surface plasmon polaritons (SPPs) using Ge nanowires;[15] Neutens et al. utilized an integrated GaAs photodetector to detect gap SPPs.[16] Direct SPP generation by electricity has also been realized through nanometer-scale light-emitting diodes using III−V semiconductors.[17−19]

Despite enormous efforts and significant progress, chip-level optical communication, i.e., the simultaneous generation and detection of SPPs, still remains a challenge. In fact, these conventional semiconductors are not the right material platform to fabricate monolithic chip-level EPIC. Taking the above-mentioned SPP devices as an example, although an SPP can be directly generated by a nanoscale integrated GaAs diode,[17,18] it can hardly be detected using the same GaAs because optical absorption at the band edge of GaAs is negligible. Two-dimensional transition metal dichalcogenides (TMDs) have recently emerged as promising nanomaterials for both electronic and photonic device applications.[20−26] TMDs such as MoS$_2$

have been used to generate or detect SPPs, but other than being atomically thin, their unique advantage of being able to emit and absorb photons at the same wavelength has not been demonstrated compared to the above-mentioned semiconductors.[27−29] Moreover, multiple exciton emissions from MoS$_2$ make the coupling of MoS$_2$ photoluminescence to SPPs of Ag waveguides unnecessarily complicated, which could hinder future device applications.

An example of Stokes shift is shown in Figure 1a. The difference in peak positions between absorption and photoluminescence spectra of ∼2 nm CdTe quantum dots is significant such that the absorption at the photoluminescence peak drops to near zero, although both absorption and photoluminescence spectra exhibit the characteristic of exciton transition. This is very different for monolayer WS$_2$.[26] Figure 1b shows the experimental setup. Large-size monolayers of WS$_2$ are synthesized by chemical vapor deposition on SiO$_2$/Si or quartz substrates.[30] Ag nanowires (AgNWs) with a diameter of ∼120 nm (AgNWs-120 from ACSMATERIAL) are used as plasmonic waveguides. A 532 nm laser is used to photoexcite the monolayer WS$_2$ through a microscope objective. For WS$_2$ on the SiO$_2$/Si substrates, the differential reflectance is measured to obtain its absorption spectrum.[31,32] Figure 1c,d show nearly perfect spectral overlaps between photoluminescence and absorption spectra of WS$_2$ monolayers on either a quartz or SiO$_2$/Si substrate. Close peak positions between absorbance and photoluminescence of WS$_2$ monolayers were also reported by Zhao[32] and Peimyoo,[33] but a bigger Stokes shift was observed by Eda and Maier.[26] Similar discrepancies among different groups can also be found for MoS$_2$,[26,31] and they are believed to be due to different crystal quality and doping levels of monolayer TMDs. Note that the shorter peak wavelength in
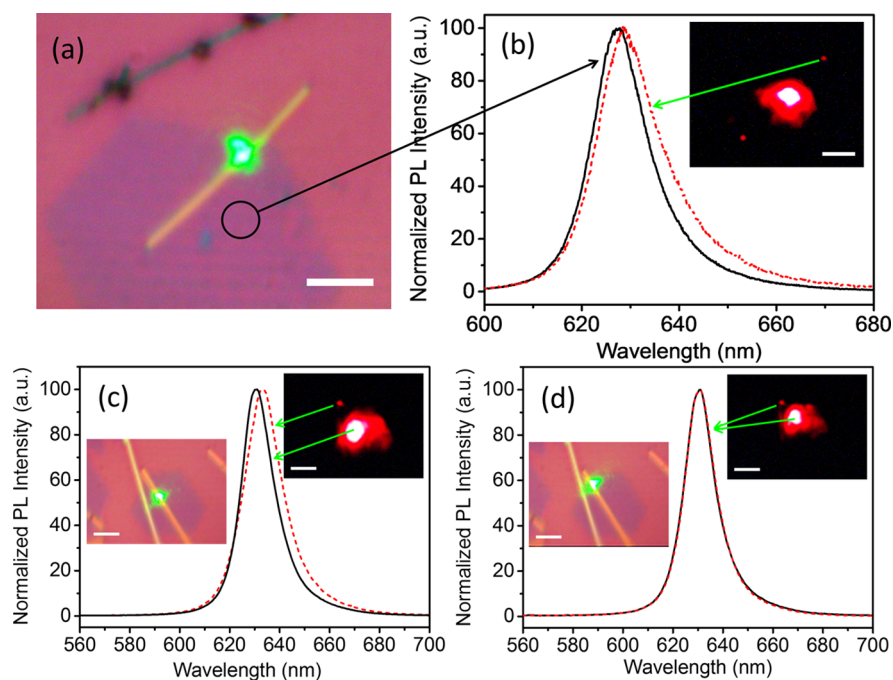
Figure 2. Spectrum of surface plasmon polaritons (SPPs) created by the photoluminescence (PL) of WS$_2$. (a) Photoexcitation image of one AgNW/WS$_2$ device. (b) Photoluminescence (black) of WS$_2$ away from the Ag nanowire and spectrum of the SPPs scattered from the silver nanowire tip (red). Inset is the associated luminescence image of the excitation image in (a). (c and d) Spectra of emitted light from the photoexcitation spot (black) and from the silver nanowire tip (red) when another device is photoexcited on AgNW/WS$_2$ (c) nearly in the middle or (d) at the edge of the WS$_2$ crystal. Insets are excitation images and the associated luminescence images. Scale bars: 3 μm. Laser wavelength: 532 nm.

Figure 1c than in Figure 1d was also observed by Peimyoo et al. due to substrate-induced strain.[33,34]

Having determined the peak wavelength of photoluminescence and established the resonance relationship between emission and absorption, we are in a position to investigate how the photoluminescence of WS$_2$ is coupled to surface plasmon polaritons and how the SPPs are subsequently absorbed by WS$_2$. Using the configuration in Figure 1b, the generation and propagation of SPPs are confirmed in Figure 2 by the appearance of red light from the ends of the Ag nanowires. Note that unlike the MoS$_2$ work, the photoluminescence spectrum remains the same no matter whether the photoexcitation is performed on bare WS$_2$ away from the nanowire or on the AgNW/WS$_2$.[27,28,35] Hence, we do not distinguish between the photoluminescence spectra from a bare WS$_2$ and from AgNW/WS$_2$, and we use either of them for convenience. On the other hand, it is not accurate to simply take the photoluminescence spectrum from AgNW/WS$_2$ as the SPP spectrum of Ag nanowires because a significant amount of photoluminescence originates directly from WS$_2$. In other words, the spectrum of coupled SPPs should be measured from the end emission of Ag nanowires, which was also used to determine the spectrum of SPPs coupled to MoS$_2$ monolayers. However, a clear red shift of SPPs can be seen in Figure 2b,c compared to the spectrum of WS$_2$, in contrast to previous work in MoS$_2$.[27,28,35]

There is always a spectral shift between the emission from the AgNW/WS$_2$ photoexcitation spot and the SPPs scattered at the AgNW end as long as the AgNW/WS$_2$ is excited inside the WS$_2$ monolayer. It is not until the photoexcitation is moved to the farthest edge of WS$_2$ and the SPPs' travel distance is short enough that the two spectra become almost identical, as shown in Figure 2d. On the basis of these observations, we can now conclude that the SPP has the same spectrum as WS$_2$

photoluminescence when it is initially created by the photoexcitation of AgNW/WS$_2$. The observations from Figure 2b,c indicate that the spectral red-shift can be induced by either a long AgNW waveguide or a combination of AgNW and WS$_2$. To find out their relative contributions, we use the same device shown in Figure 2a and move the photoexcitation spot more into WS$_2$. Figure 3a,b show the SPP travels toward both ends 1A and 1B of the nanowire. Despite a longer travel distance to 1B, the SPP from 1A experiences more red-shift than that from 1B, as revealed in Figure 3e. This observation leads us to conclude that SPP interaction with WS$_2$ has a more significant contribution to its spectral red-shift.

The effect of WS$_2$ and Ag nanowire on the spectral red-shift of SPPs can also be seen in Figure 3b, c, d, and f, when WS$_2$ is photoexcited at different locations along the Ag nanowire. A larger spectral shift is observed when the propagation distance along AgNW/WS$_2$ increases. Moreover, the spectral shift is accompanied by a decreasing intensity of the SPPs. Because the photoexcitation must be performed over AgNW/WS$_2$, simultaneous propagation losses from both the Ag nanowire and WS$_2$ cannot be avoided. In order to distinguish these two propagation losses and investigate their underlying loss mechanisms, we normalize the spectrum of SPPs with respect to the photoluminescence spectrum of WS$_2$. As can be seen from Figure 3g, both SPP spectra exhibit a gradual decrease in spectral loss at longer wavelengths and a resonant absorption, but the resonant absorption in spectrum 1A is more pronounced than that of 1B. We attribute the broad absorption to the SPP propagation loss from AgNW/WS$_2$[36] and the resonant absorption to WS$_2$. This conclusion agrees with the absorption spectrum of WS$_2$ in Figure 1, where a strong resonant absorption peak is superposed on the broadband background. The weaker WS$_2$ absorption for 1B SPP is due to its shorter interaction length with WS$_2$ because less than half of the distance is above the WS$_2$. To obtain a better
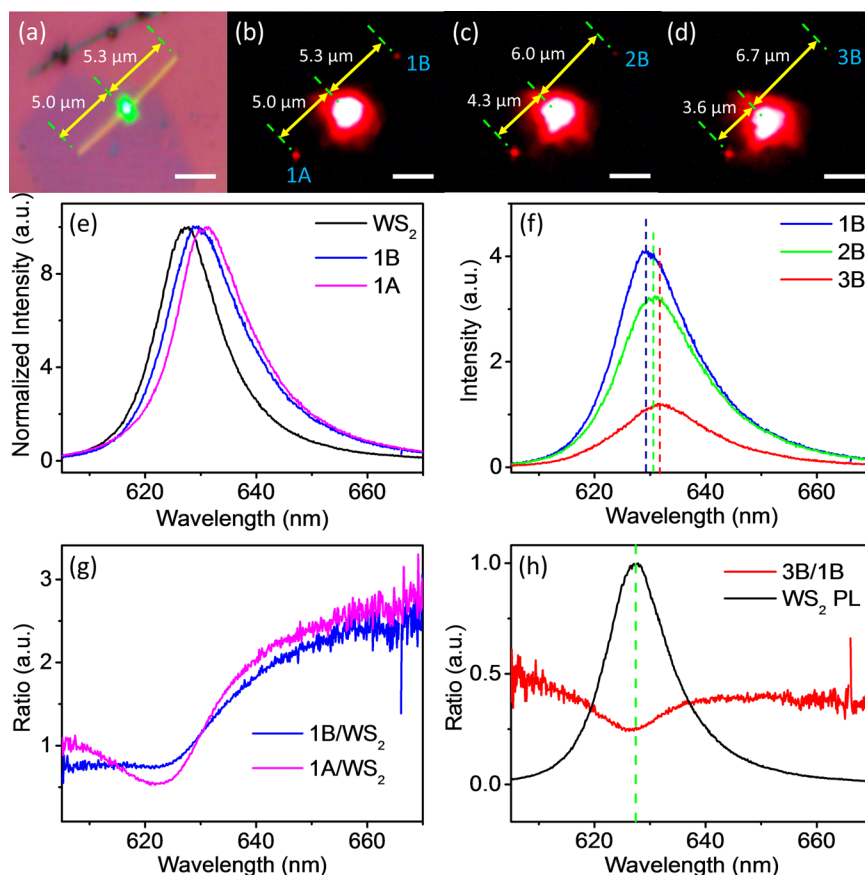
Figure 3. Absorption spectrum of surface plasmon polaritons (SPPs) by WS$_2$. (a) Excitation image of the device. (b) Luminescence image of (a). (c and d) Luminescence images when WS$_2$ is photoexcited at two other locations along the Ag nanowire. (e) Normalized spectra of the photoexcitation (black) and SPPs from points 1A and 1B in part (b). (f) SPP spectra from 1B, 2B, and 3B in parts (b)−(d). (g) Ratios of the spectra 1B and 1A to the exciton spectrum of WS$_2$. (h) Ratio of spectrum 3B to spectrum 1B (red), in comparison to the spectrum of WS$_2$. Scale bars: 3 μm.
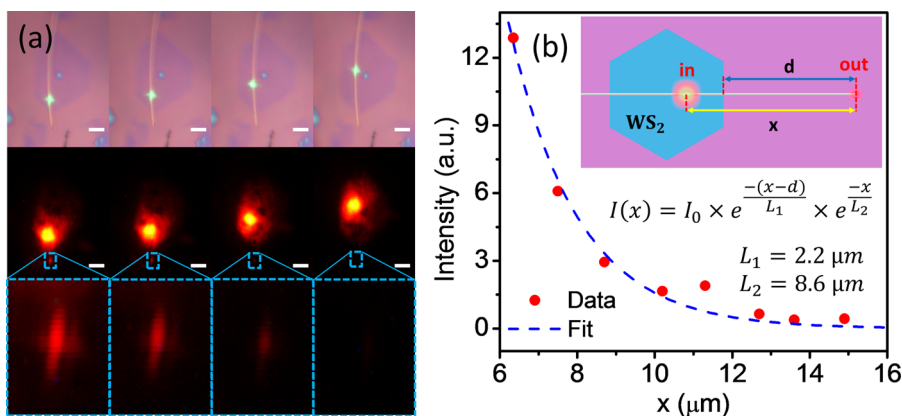

Figure 4. Measurement of SPP propagation length. (a) Photoexcitation (top) and SPP emission images (zoomed-in images at the bottom). (b) Intensity of the SPP based on (a) as a function of propagation length. Inset: Schematic of the experimental design. Scale bars: 5 μm.

resonant absorption spectrum with less broadband absorption background, we normalized the spectrum of 3B using the spectrum of 1B as a reference; the result in Figure 3h shows a clear resonance with the reduced propagation loss from the nanowire. We also include the photoluminescence in the same plot, and an excellent overlap is observed. Thus, we can conclude that the SPP is resonantly absorbed by WS$_2$ at the same wavelength as the photoluminescence; there is no difference between the SPP and free-space light when it interacts with WS$_2$; over a short distance of less than 2 μm, the

propagation loss of the SPP is dominated by resonant absorption of WS$_2$.

To quantify the resonant absorption of SPP by WS$_2$, we selected a device with a longer Ag nanowire both on and outside of WS$_2$ so that the SPP propagation distance can be varied in a wider range. Figure 4 shows the experimental design and calculation principle. When an SPP is created by photoexcitation, it will go through two regions before reaching the clear end of the nanowire waveguide: the first region is the nanowire on WS$_2$, and the second one is the nanowire alone. We
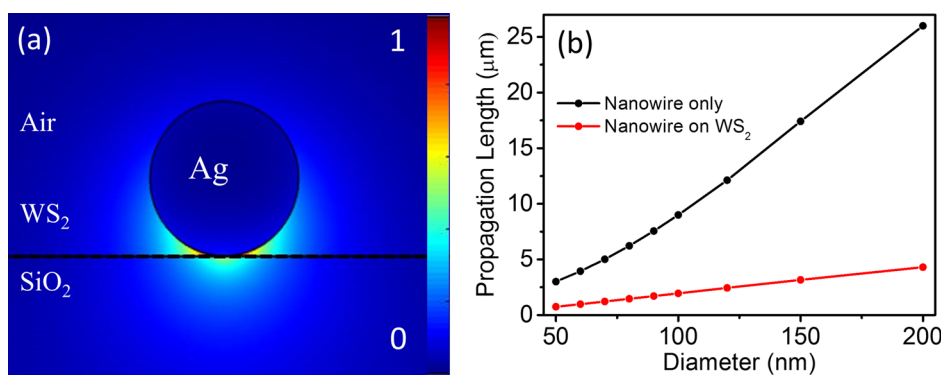
Figure 5. Numerical calculation of SPP propagation length. (a) Cross-sectional view of a field intensity profile of a propagating SPP at 633 nm. The diameter of the nanowire is 120 nm. (b) Calculated SPP propagation lengths along the Ag nanowire as a function of the nanowire diameter with and without WS_2.

designate α_1 and α_2 as the absorption coefficients due to WS_2 and the nanowire, respectively. The total absorption coefficient when the nanowire on WS_2 can be approximated as $\alpha_1 + \alpha_2$. Thus, the intensity of SPP end emission at the point x can be expressed as

$$I(x) = I_o e^{-(\alpha_1+\alpha_2)(x-d)} e^{-\alpha_2 d} = I_o e^{-\alpha_1(x-d)} e^{-\alpha_2 x} \qquad (1)$$

Here I_0 is the intensity of the exciton SPP at the point of photoexcitation. If we define propagation length L_1 and L_2 as $L_1 = 1/\alpha_1$, $L_2 = 1/\alpha_2$, then the equation can be written as

$$I(x) = I_o e^{-(\alpha_1+\alpha_2)(x-d)} e^{-\alpha_2 d} = I_o e^{-(x-d)/L_1} e^{-x/L_2} \qquad (2)$$

The propagation lengths L_1 and L_2 can be obtained by curve fitting eq 2. Figure 4a shows a series of snapshots of SPP photoexcitation and SPP end emission. The integrated SPP intensity is plotted in Figure 4b as a function of SPP travel distance. Curve fitting by eq 2 gives us $L_1 = 2.2$ μm and $L_2 = 8.6$ μm. The propagation length L of SPP with the nanowire on WS_2 is ~1.8 μm based on the total absorption of $\alpha_1 + \alpha_2$. The propagation L_2 is similar to previously reported values using silver nanowires with a similar diameter.[36−40] We also measured the propagation length of a silver nanowire fully placed on a WS_2 crystal. In that case, we obtain $L_1 = 2.4$ μm, $L_2 = 12.2$ μm, and the propagation length $L = 2.0$ μm.

The understanding of SPP absorption allows us to numerically calculate the propagation length based on the measured optical constants of WS_2.[41] Note that the strong absorption of SPPs by a WS_2 monolayer is also a result of plasmon-enhanced strong light−matter interaction. Figure 5a shows the local field distribution around the AgNW/WS_2 at 633 nm, which is close to the wavelength of WS_2 SPPs. This is the fundamental mode of an SPP, and it has been previously studied without a WS_2 monolayer.[39,40,42] Although only one monolayer thick, the effect of monolayer WS_2 is noticeable: the field becomes more concentrated in the region where the nanowire and WS_2 overlap, leading to a short propagation length. Figure 5b shows the dependence of SPP propagation length on nanowire diameter with and without WS_2. It can be seen that the effect of WS_2 is strong regardless of the nanowire's diameter. For the 120 nm nanowire, we obtain a propagation length of 2.4 μm, which is in good agreement with the experimental value.

The well-defined photoluminescence and absorption peaks as well as their excellent spectral overlap are a result of excitonic transitions in WS_2 monolayers and are a general property of monolayer TMDs.[26,31,33,43,44] A large exciton binding energy in monolayer TMDs enables a discrete absorption spectrum.[31,43,44] The SPP wavelength can be selected by choosing different TMDs or tuned by straining or doping.[34] Here chemically synthesized Ag nanowires are used only to demonstrate the concept, and lithographically defined plasmonic waveguides and couplers could be used for large-scale integration.[19,38]

In conclusion, we have demonstrated optical emission and absorption resonance not only for free-space light but also for surface plasmon polaritons. The same resonant wavelength of photon emission and absorption is determined by direct exciton transitions in monolayer TMDs. Although the generation and detection of SPPs were demonstrated optically, the device can be readily modified to perform local generation and detection of SPPs by electrical means, i.e., nanoscale optical communication between transistors on the same chip. Because the planar structure of 2D TMDs is compatible with the current lithographic fabrication process, we expect the demonstration of a complete EPIC in the not too distant future.

■ AUTHOR INFORMATION

Corresponding Authors
*E-mail: jbao@uh.edu.
*E-mail: zhmwang@uestc.edu.cn.

Notes
The authors declare no competing financial interest.

■ REFERENCES

(1) Chou, K. F.; Dennis, A. M. Forster Resonance Energy Transfer between Quantum Dot Donors and Quantum Dot Acceptors. *Sensors* **2015**, *15*, 13288−13325.

(2) Efros, A. L.; Rosen, M.; Kuno, M.; Nirmal, M.; Norris, D. J.; Bawendi, M. Band-edge exciton in quantum dots of semiconductors with a degenerate valence band: Dark and bright exciton states. *Phys. Rev. B: Condens. Matter Mater. Phys.* **1996**, *54*, 4843−4856.

(3) Li, J. B.; Xia, J. B. Exciton states and optical spectra in CdSe nanocrystallite quantum dots. *Phys. Rev. B: Condens. Matter Mater. Phys.* **2000**, *61*, 15880−15886.

(4) Bagga, A.; Chattopadhyay, P. K.; Ghosh, S. Origin of Stokes shift in InAs and CdSe quantum dots: Exchange splitting of excitonic states. *Phys. Rev. B: Condens. Matter Mater. Phys.* **2006**, *74*, 035341.

(5) Seidl, S.; Kroner, M.; Dalgarno, P. A.; Hogele, A.; Smith, J. M.; Ediger, M.; Gerardot, B. D.; Garcia, J. M.; Petroff, P. M.; Karrai, K.; Warburton, R. J. Absorption and photoluminescence spectroscopy on a single self-assembled charge-tunable quantum dot. *Phys. Rev. B: Condens. Matter Mater. Phys.* **2005**, *72*, 195339.

(6) Heck, M. J. R.; Bauters, J. F.; Davenport, M. L.; Doylend, J. K.; Jain, S.; Kurczveil, G.; Srinivasan, S.; Tang, Y. B.; Bowers, J. E. Hybrid Silicon Photonic Integrated Circuit Technology. *IEEE J. Sel. Top. Quantum Electron.* **2013**, *19*, 6100117.

(7) Ahn, D.; Hong, C. Y.; Liu, J. F.; Giziewicz, W.; Beals, M.; Kimerling, L. C.; Michel, J.; Chen, J.; Kartner, F. X. High performance, waveguide integrated Ge photodetectors. *Opt. Express* **2007**, *15*, 3916−3921.

(8) Politi, A.; Cryan, M. J.; Rarity, J. G.; Yu, S. Y.; O'Brien, J. L. Silica-on-silicon waveguide quantum circuits. *Science* **2008**, *320*, 646−649.

(9) Estevez, M. C.; Alvarez, M.; Lechuga, L. M. Integrated optical devices for lab-on-a-chip biosensing applications. *Laser Photon. Rev.* **2012**, *6*, 463−487.

(10) Sun, C.; Wade, M. T.; Lee, Y.; Orcutt, J. S.; Alloatti, L.; Georgas, M. S.; Waterman, A. S.; Shainline, J. M.; Avizienis, R. R.; Lin, S.; Moss, B. R.; Kumar, R.; Pavanello, F.; Atabaki, A. H.; Cook, H. M.; Ou, A. J.; Leu, J. C.; Chen, Y. H.; Asanovic, K.; Ram, R. J.; Popovic, M. A.; Stojanovic, V. M. Single-chip microprocessor that communicates directly using light. *Nature* **2015**, *528*, 534−538.

(11) Dickson, R. M.; Lyon, L. A. Unidirectional plasmon propagation in metallic nanowires. *J. Phys. Chem. B* **2000**, *104*, 6095−6098.

(12) Atwater, H. A.; Maier, S.; Polman, A.; Dionne, J. A.; Sweatlock, L. The new ″p−n junction″. Plasmonics enables photonic access to the nanoworld. *MRS Bull.* **2005**, *30*, 385−389.

(13) Barnes, W. L.; Dereux, A.; Ebbesen, T. W. Surface plasmon subwavelength optics. *Nature* **2003**, *424*, 824−830.

(14) Ozbay, E. Plasmonics: Merging photonics and electronics at nanoscale dimensions. *Science* **2006**, *311*, 189−193.

(15) Falk, A. L.; Koppens, F. H. L.; Yu, C. L.; Kang, K.; Snapp, N. D.; Akimov, A. V.; Jo, M. H.; Lukin, M. D.; Park, H. Near-field electrical detection of optical plasmons and single-plasmon sources. *Nat. Phys.* **2009**, *5*, 475−479.

(16) Neutens, P.; Van Dorpe, P.; De Vlaminck, I.; Lagae, L.; Borghs, G. Electrical detection of confined gap plasmons in metal-insulator-metal waveguides. *Nat. Photonics* **2009**, *3*, 283−286.

(17) Fan, P. Y.; Colombo, C.; Huang, K. C. Y.; Krogstrup, P.; Nygard, J.; Morral, A. F. I.; Brongersma, M. L. An Electrically-Driven GaAs Nanowire Surface Plasmon Source. *Nano Lett.* **2012**, *12*, 4943−4947.

(18) No, Y. S.; Choi, J. H.; Ee, H. S.; Hwang, M. S.; Jeong, K. Y.; Lee, E. K.; Seo, M. K.; Kwon, S. H.; Park, H. G. A Double-Strip Plasmonic Waveguide Coupled to an Electrically Driven Nanowire LED. *Nano Lett.* **2013**, *13*, 772−776.

(19) Huang, K. C. Y.; Seo, M. K.; Sarmiento, T.; Huo, Y. J.; Harris, J. S.; Brongersma, M. L. Electrically driven subwavelength optical nanocircuits. *Nat. Photonics* **2014**, *8*, 244−249.

(20) Cheng, R.; Jiang, S.; Chen, Y.; Liu, Y.; Weiss, N.; Cheng, H. C.; Wu, H.; Huang, Y.; Duan, X. F. Few-layer molybdenum disulfide transistors and circuits for high-speed flexible electronics. *Nat. Commun.* **2014**, *5*, 5143.

(21) Radisavljevic, B.; Radenovic, A.; Brivio, J.; Giacometti, V.; Kis, A. Single-layer MoS2 transistors. *Nat. Nanotechnol.* **2011**, *6*, 147−150.

(22) Wang, Q. H.; Kalantar-Zadeh, K.; Kis, A.; Coleman, J. N.; Strano, M. S. Electronics and optoelectronics of two-dimensional transition metal dichalcogenides. *Nat. Nanotechnol.* **2012**, *7*, 699−712.

(23) Koppens, F. H. L.; Mueller, T.; Avouris, P.; Ferrari, A. C.; Vitiello, M. S.; Polini, M. Photodetectors based on graphene, other two-dimensional materials and hybrid systems. *Nat. Nanotechnol.* **2014**, *9*, 780−793.

(24) Pospischil, A.; Furchi, M. M.; Mueller, T. Solar-energy conversion and light emission in an atomic monolayer p-n diode. *Nat. Nanotechnol.* **2014**, *9*, 257−261.

(25) Baugher, B. W. H.; Churchill, H. O. H.; Yang, Y. F.; Jarillo-Herrero, P. Optoelectronic devices based on electrically tunable p-n diodes in a monolayer dichalcogenide. *Nat. Nanotechnol.* **2014**, *9*, 262−267.

(26) Eda, G.; Maier, S. A. Two-Dimensional Crystals: Managing Light for Optoelectronics. *ACS Nano* **2013**, *7*, 5660−5665.

(27) Goodfellow, K. M.; Beams, R.; Chakraborty, C.; Novotny, L.; Vamivakas, A. N. Integrated nanophotonics based on nanowire plasmons and atomically thin material. *Optica* **2014**, *1*, 149−152.

(28) Lee, H. S.; Kim, M. S.; Jin, Y.; Han, G. H.; Lee, Y. H.; Kim, J. Efficient Exciton-Plasmon Conversion in Ag Nanowire/Monolayer MoS2 Hybrids: Direct Imaging and Quantitative Estimation of Plasmon Coupling and Propagation. *Adv. Opt. Mater.* **2015**, *3*, 943−947.

(29) Goodfellow, K. M.; Chakraborty, C.; Beams, R.; Novotny, L.; Vamiyakas, A. N. Direct On-Chip Optical Plasmon Detection with an Atomically Thin Semiconductor. *Nano Lett.* **2015**, *15*, 5477−5481.

(30) Cong, C. X.; Shang, J. Z.; Wu, X.; Cao, B. C.; Peimyoo, N.; Qiu, C.; Sun, L. T.; Yu, T. Synthesis and Optical Properties of Large-Area Single-Crystalline 2D Semiconductor WS₂ Monolayer from Chemical Vapor Deposition. *Adv. Opt. Mater.* **2014**, *2*, 131−136.

(31) Mak, K. F.; Lee, C.; Hone, J.; Shan, J.; Heinz, T. F. Atomically Thin MoS₂: A New Direct-Gap Semiconductor. *Phys. Rev. Lett.* **2010**, *105*, 136805.

(32) Zhao, W. J.; Ghorannevis, Z.; Chu, L. Q.; Toh, M. L.; Kloc, C.; Tan, P. H.; Eda, G. Evolution of Electronic Structure in Atomically Thin Sheets of WS₂ and WSe₂. *ACS Nano* **2013**, *7*, 791−797.

(33) Peimyoo, N.; Shang, J. Z.; Cong, C. X.; Shen, X. N.; Wu, X. Y.; Yeow, E. K. L.; Yu, T. Nonblinking, Intense Two-Dimensional Light Emitter: Mono layer WS₂ Triangles. *ACS Nano* **2013**, *7*, 10985−10994.

(34) Shi, H. L.; Pan, H.; Zhang, Y. W.; Yakobson, B. I. Quasiparticle band structures and optical properties of strained monolayer MoS₂ and WS₂. *Phys. Rev. B: Condens. Matter Mater. Phys.* **2013**, *87*, 155304.

(35) Lee, H. S.; Kim, M. S.; Jin, Y.; Han, G. H.; Lee, Y. H.; Kim, J. Selective Amplification of the Primary Exciton in a MoS₂ Monolayer. *Phys. Rev. Lett.* **2015**, *115*, 226801.

(36) Yan, R. X.; Pausauskie, P.; Huang, J. X.; Yang, P. D. Direct photonic-plasmonic coupling and routing in single nanowires. *Proc. Natl. Acad. Sci. U. S. A.* **2009**, *106*, 21045−21050.

(37) Ditlbacher, H.; Hohenau, A.; Wagner, D.; Kreibig, U.; Rogers, M.; Hofer, F.; Aussenegg, F. R.; Krenn, J. R. Silver nanowires as surface plasmon resonators. *Phys. Rev. Lett.* **2005**, *95*, 257403.

(38) Kusar, P.; Gruber, C.; Hohenau, A.; Krenn, J. R. Measurement and Reduction of Damping in Plasmonic Nanowires. *Nano Lett.* **2012**, *12*, 661−665.

(39) Wei, H.; Xu, H. X. Nanowire-based plasmonic waveguides and devices for integrated nanophotonic circuits. *Nanophotonics* **2012**, *1*, 155−169.

(40) Guo, X.; Ma, Y. G.; Wang, Y. P.; Tong, L. M. Nanowire plasmonic waveguides, circuits and devices. *Laser Photon. Rev.* **2013**, *7*, 855−881.

(41) Li, S. L.; Miyazaki, H.; Song, H.; Kuramochi, H.; Nakaharai, S.; Tsukagoshi, K. Quantitative Raman Spectrum and Reliable Thickness Identification for Atomic Layers on Insulating Substrates. *ACS Nano* **2012**, *6*, 7381−7388.

(42) Qian, H. L.; Ma, Y. G.; Yang, Q.; Chen, B. G.; Liu, Y.; Guo, X.; Lin, S. S.; Ruan, J. L.; Liu, X.; Tong, L. M.; Wang, Z. L. Electrical Tuning of Surface Plasmon Polariton Propagation in Graphene-Nanowire Hybrid Structure. *ACS Nano* **2014**, *8*, 2584−2589.

(43) Ramasubramaniam, A. Large excitonic effects in monolayers of molybdenum and tungsten dichalcogenides. *Phys. Rev. B: Condens. Matter Mater. Phys.* **2012**, *86*, 115409.

(44) Chernikov, A.; Berkelbach, T. C.; Hill, H. M.; Rigosi, A.; Li, Y. L.; Aslan, O. B.; Reichman, D. R.; Hybertsen, M. S.; Heinz, T. F. Exciton Binding Energy and Nonhydrogenic Rydberg Series in Monolayer WS₂. *Phys. Rev. Lett.* **2014**, *113*, 076802.